



ELSEVIER

Contents lists available at [SciVerse ScienceDirect](http://www.sciencedirect.com)

Biosensors and Bioelectronics

journal homepage: www.elsevier.com/locate/bios

X-ray enabled detection and eradication of circulating tumor cells with nanoparticles

Mainul Hossain^{a,b,1}, Yang Luo^{a,c,1}, Zhaoyong Sun^a, Chaoming Wang^a, Minghui Zhang^{a,d}, Hanyu Fu^a, Yong Qiao^a, Ming Su^{a,b,*}

^a NanoScience Technology Center, University of Central Florida, Orlando, FL 32826 USA

^b School of Electrical Engineering and Computer Science, University of Central Florida, Orlando, FL 32826 USA

^c Department of Laboratory Medicine, Southwest Hospital, Third Military Medical University, Chongqing 400038, China

^d Key Laboratory of Advanced Energy Materials Chemistry (MOE), College of Chemistry, Nankai University, Tianjin 300071 China

ARTICLE INFO

Article history:

Received 3 April 2012

Received in revised form

14 May 2012

Accepted 13 June 2012

Available online 23 June 2012

Keywords:

Circulating tumor cells

Capture

Detection

Localization

Nanoparticles

ABSTRACT

The early detection and eradication of circulating tumor cells (CTCs) play an important role in cancer metastasis management. This paper describes a new nanoparticle-enabled technique for integrated enrichment, detection and killing of CTCs by using magnetic nanoparticles and bismuth nanoparticles, X-ray fluorescence spectrometry, and X-ray radiation. The nanoparticles are modified with tumor targeting agents and conjugated with tumor cells through folate receptors over-expressed on cancer cells. A permanent micro-magnet is used to collect CTCs suspended inside a flowing medium that contains phosphate buffered saline (PBS) or whole blood. The characteristic X-ray emissions from collected bismuth nanoparticles, upon excitation with collimated X-rays, are used to detect CTCs. Results show that the method is capable of selectively detecting CTCs at concentrations ranging from 100–100,000 cells/mL in the buffer solution, with a detection limit of ~100 CTCs/mL. Moreover, the dose of primary X-rays can be enhanced to kill the localized CTCs by radiation induced DNA damage, with minimal invasiveness, thus making *in vivo* personalized CTC management possible.

© 2012 Elsevier B.V. All rights reserved.

1. Introduction

Early diagnosis and treatment of cancer are highly important for reducing mortality and recurrence probability (Wulfkühle et al., 2003). The five year survival rate of patients with localized breast cancers is 95%, while that of patients with metastatic cancer reduces to 30%, which highlights the importance of early detection in cancer management (Heimann and Hellman, 2000). Detecting circulating tumor cells (CTCs) released inside blood stream of patients during cancer development could provide a sensitive and minimally invasive way to monitor cancer progress

Abbreviation: APTES, (3-aminopropyl)-triethoxysilane; CTC, Circulating tumor cells; DLS, Dynamic light scattering; DMF, N,N dimethylformamide; DMSO, Dimethylsulfoxide; D-PBS, Dulbecco's phosphate-buffered saline; EB, Ethidium bromide; EDC, Ethyl-3-(3-dimethylaminopropyl) carbodiimide; EDTA, Ethylenediaminetetraacetic acid; FBS, Fetal bovine serum; FA, Folic acid; FA-Bi, Folic acid conjugated bismuth nanoparticles; FR, Folate receptor; FTIR, Fourier transform infrared spectroscopy; MTT, 3(4,5-dimethylthiazol)-2-diphenyltertrazolium bromide; PBS, Phosphate-buffered saline; PVP, Poly(vinylpyrrolidone); SNR, Signal-to-noise ratio; TEM, Transmission electron microscope; XRF, X-ray fluorescence

* Corresponding author at: NanoScience Technology Center, University of Central Florida, Orlando, FL 32826 USA.

E-mail address: mingsu@mail.ucf.edu (M. Su).

¹ M. Hossain and Y. Luo contributed equally to this work.

0956-5663/\$ - see front matter © 2012 Elsevier B.V. All rights reserved.

<http://dx.doi.org/10.1016/j.bios.2012.06.020>

(Kaiser, 2010; Liu et al., 2009; Nezos et al., 2011; Sun et al., 2011). But, it is challenging to detect CTCs in blood, because CTCs in early stage cancer patients are extremely rare (1 CTC in 7.5 mL of blood or 1 CTC against 10^3 – 10^7 nucleated cells in blood) (Yu et al., 2011). An enrichment step is required prior to CTC detection (Pantel et al., 2008; Zemp, 2009). Many techniques have been used for CTC enrichment such as microfluidic CTC chips (Dharmasiri et al., 2011; He et al., 2007; Nagrath et al., 2007; Wang et al., 2011a), magnetic particles (Benez et al., 1999; Bilkenroth et al., 2001; Zborowski and Chalmers, 2011), micro-filtration (Lin et al., 2010; Zheng et al., 2007; Zheng et al., 2011), dielectric separation (Gascoyne et al., 2009), and flow cytometry (Georgakoudi et al., 2004; Hu et al., 2010; Zharov et al., 2006). These methods are dependent on physical properties of tumor cells (size, mechanical stiffness, or dielectric property), or surface receptors over-expressed on tumor surfaces. Once collected, CTCs can be detected with fluorescence method (Hsieh et al., 2006; Kojima et al., 2009), photoacoustic method (Galanzha et al., 2009; Gutierrez-Juarez et al., 2010; Nedosekin et al., 2010; Weight et al., 2006), electrical method (Chung et al., 2011), flow cytometry, cell counting, and Raman spectroscopy (Neugebauer et al., 2010; Sha et al., 2008; Wang et al., 2011b). Though these methods have shown the prospects of CTCs in cancer management, existing CTC techniques are limited for few reasons: (1) CTC numbers detected

by different methods vary drastically from several to several hundred, which can be partly due to tumor heterogeneity in patient and complex nature of blood, but is more likely due to variation in collection or detection efficiency of different methods; (2) CTC detection has not been seamlessly integrated with treatment, thus patients will have to wait for certain time before treatment starts, which can lead to tumor metastasis to distant organ; (3) chemotherapy is often used for CTC treatments, but drugs used in chemotherapy are toxic to normal cells, and there is no localized treatment option available for CTCs. If CTCs could be killed locally and non-invasively, damage to normal cells will be minimized, and there is no need to use invasive treatments such as surgery. Nanostructured materials (*i.e.*, golden carbon nanotubes and magnetic nanoparticles) have been used in combination to capture and detect CTCs, but the method needs complicated photoacoustic devices for CTC detection, and tumor killing is not integrated (Galanzha et al., 2009). CTC detections have also been achieved *in vivo* using flow cytometry after labeling CTCs with fluorescent probes that target surface receptors of CTCs (He et al., 2007), but the method does not take CTC removal or elimination into consideration.

X-ray fluorescence (XRF) has been used to detect multiple DNA and protein biomarkers by using metallic nanoparticles as probes (Hossain et al., 2010). XRF spectrometry is a widely used analytical method for detecting trace elements in various samples due to its high sensitivity, specificity and simplicity (Hatzistavros et al. (2007); Mann et al., 2000). The characteristic X-ray emissions from elements, present in the X-ray irradiated samples, are detected using an X-ray spectrometer. The amount of each element present in the sample can be quantified based on the intensity of according XRF peak. Bismuth nanoparticles are promising candidates for biomarker detection, cancer imaging and therapy due to bismuth's large atomic number (83) and relatively low toxicity (Rabin et al., 2006). Meanwhile, superparamagnetic iron oxide nanoparticles are well known for their enrichment capability and biocompatibility and have been widely applied in detection of rare analytes (Bhattacharya et al., 2011). This paper describes an integrated method that can be used for *in vivo* CTC management by combining magnetic nanoparticle based capture, XRF based detection and X-ray radiation killing of CTCs. The feasibility of this integrated approach has been confirmed in this proof-of-concept *in vitro* experiment: superparamagnetic iron oxide nanoparticles and X-ray absorbing bismuth nanoparticles are modified by folic acid (FA) ligands that bind to folate receptors (FR) over-expressed on tumor cell surfaces; after adding both nanoparticles in cell suspension, nanoparticles can bind on surfaces of tumor cells; a micro-magnet allows localization of CTCs in a small area (preferentially underneath the skin in case of *in vivo* detection); an incoming X-ray beam excites the characteristic X-rays of bismuth nanoparticles, signaling the presence of CTCs; subsequently, X-ray intensity can be increased to damage DNA of CTCs and kill CTCs locally (Fig. 1).

2. Materials and methods

2.1. Materials

HeLa (CLL-2) and MG-63 (CRL-1427) cell lines are obtained from American Type Culture Collection (ATCC, Manassas, VA). 3(4,5-dimethylthiazol)-2-diphenyltertrazolium bromide (MTT) kit for mammalian cells is supplied by Invitrogen (Carlsbad, CA). Single donor human whole blood containing anticoagulant of ethylenediaminetetraacetic acid (EDTA) is obtained from Innovative Research (Novi, MI). FA is obtained from VWR (West Chester, PA). Hydrated bismuth nitrate ($\text{Bi}(\text{NO}_3)_3 \cdot 5\text{H}_2\text{O}$), sodium borohydride (NaBH_4),

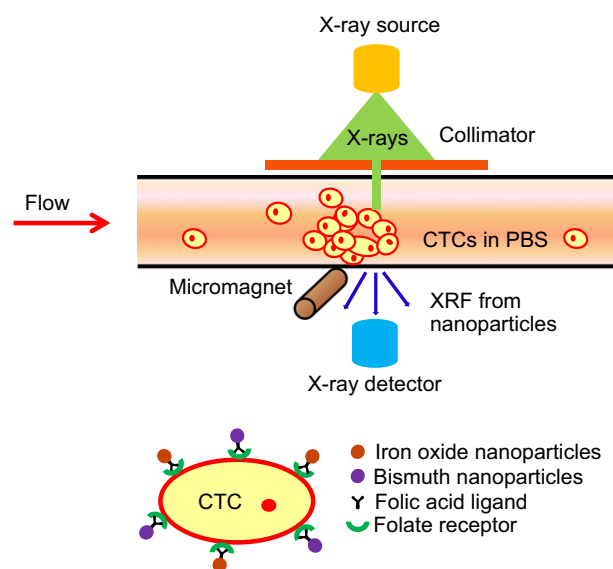


Fig. 1. Nanoparticle enabled integrated enrichment, detection and killing of circulating tumor cells.

RPMI 1640 culture media, penicillin, streptomycin, fetal bovine serum (FBS), and Dulbecco's phosphate-buffered saline (D-PBS) are from Sigma-Aldrich (St. Louis, MO). Ultrapure water ($18.2 \text{ M}\Omega \text{ cm}^{-1}$) from Nanopure System (Barnstead, Kirkland, WA) is used throughout. All the other chemicals are obtained from VWR (West Chester, PA) and used as received.

2.2. Nanoparticle synthesis

Iron oxide nanoparticles are synthesized as follows: 1 mmol of $\text{Fe}(\text{acac})_3$ and 4 mmol of 1,2-dodecanediol are dissolved into a mixture of 10 mL of benzyl ether, 3 mL of oleic acid and 1 mL of oleylamine. The mixture is then dehydrated at 110°C under argon flow for 1 h, and heated up to 200°C for 30 min, and at 290°C for 2.5 h. After cooling to room temperature, 30 mL of anhydrous ethanol is added in the mixture to separate nanoparticles. The nanoparticles collected by centrifugation (7000 rpm, 10 min) are washed with ethanol and dispersed in hexane. After precipitated with acetone, the nanoparticles are dispersed in 1 mol/L ammonia in isopropanol, sonicated for 30 min, centrifuged, and washed with acetone, toluene and ethanol to remove oleic acid and oleylamine.

Bismuth nanoparticles are made as follows: 0.1 mmol of $\text{Bi}(\text{NO}_3)_3$ and 0.5 mmol of poly(vinylpyrrolidone) (PVP) are dissolved in 10 mL of N,N-dimethylformamide (DMF). The mixture is degassed with argon for 15 min under stirring. 0.3 mL of 1 mol/L NaBH_4 in water is mixed with 10 mL of DMF and added in the mixture of $\text{Bi}(\text{NO}_3)_3$ and PVP under vigorous stirring and argon flow for 5 min. The nanoparticles are precipitated by adding acetone, followed by centrifugation, washing with acetone and drying in vacuum. A JEOL 1011 transmission electron microscope (TEM) operated at 100 kV is used to derive the size and shape of the synthesized nanoparticles.

2.3. Conjugation of nanoparticles with folic acid

The conjugation of FA with iron oxide nanoparticles and bismuth nanoparticles is carried out as follows (Zhang et al., 2002): both nanoparticles are washed twice in ethanol, centrifuged, dried at 110°C for 1 h, and vacuum-dried overnight to remove adsorbed water. 15 mg of dried nanoparticles are dispersed in 3 mmol/L (3-aminopropyl)-triethoxysilane (APTES) in

5 mL toluene. The mixture is sonicated and incubated at 60 °C for 4 h. The suspension is centrifuged, and the precipitates are sonicated in toluene for 10 min, and washed with toluene and ethanol. The precipitates are then added to the mixture of 1 mL of 10 mmol/L FA solution in 500 μ L of dimethylsulfoxide (DMSO), 1.5 mL of 15 mmol/L N-hydroxysuccinimide (NHS), and 1.5 mL of 75 mmol/L 1-ethyl-3-(3-dimethylaminopropyl) carbodiimide (EDC) solution in water, using triethylamine as a catalyst. After adjusting pH to 9 and incubation at 37 °C for 4 h, the suspension is centrifuged, and precipitate is washed with deionized water and vacuum-dried overnight. FA-modified nanoparticles are redispersed in phosphate buffered saline (PBS) to 1 mg/mL, and stored in refrigerator. The hydrodynamic diameter of FA conjugated nanoparticles in PBS is measured by dynamic light scattering (DLS) with PD2000 DLS detector. The covalent bonding of FA with the nanoparticles is confirmed using Fourier transform infrared spectroscopy (FTIR).

2.4. Cell culture and nanoparticles treatment

Human adenocarcinoma HeLa cells and human osteosarcoma MG-63 cells are cultured in 75 cm² flasks that contain 15 mL RPMI-1640 medium supplemented with 10% FBS and 5% penicillin at 37 °C with 5% CO₂. When cells become 80% confluence, an equimolar mixture of 100 μ g/mL of FA-conjugated iron oxide nanoparticles in PBS ($\sim 10^{13}$ particles/mL) and 100 μ g/mL of FA conjugated bismuth nanoparticles in PBS ($\sim 10^{11}$ particles/mL) is added to the petri dish containing the cultured cells ($\sim 1 \times 10^5$). After incubating for 24 h (37 °C and 5% CO₂), the cells are rinsed five times in PBS to remove any unbound or non-specifically bound nanoparticles. The cells are then detached from flasks by incubating with trypsin-EDTA solution at 37 °C for 5 min, followed by centrifugation at 1000 rpm for 8 min, before being redispersed in PBS and introduced into an *in vitro* circulating system designed to mimic human blood flow.

2.5. Setup for CTC capture, detection and killing

A Mini-X portable X-ray tube (Amptek, Bedford, MA) with a silver anode operating at 30 kV and 15 μ A is used to produce primary X-rays. The tube is fitted with a series of brass and tungsten collimators to reduce outgoing beam size from 2 mm to 400 μ m in diameter. An X-ray spectrometer (Amptek X-123) with Si-PIN photodiode is used to analyze XRF emissions in the transmission mode. The X-ray spectrometer contains a solid-state detector, a digital pulse processor and a multichannel analyzer, which are interfaced with a computer for data acquisition and analysis. A 25 μ m thick silver filter and a 250 μ m thick aluminum filter are used in combination to reduce background and improve signal-to-noise ratio (SNR) in low energy region (0–15 keV) of the XRF spectrum. A neodymium–iron–boron micro-magnet obtained from BJA Magnetics (Leominster, MA) with diameter of 300 μ m, length of 2.5 mm and field strength of 0.5 mT is attached onto one side of a polyethylene tube of 1 mm inner diameter. The distance between X-ray source and the tube, and that between the tube and detector are 2 and 1 cm, respectively. HeLa cells ($\sim 1 \times 10^5$) containing FA conjugated bismuth nanoparticles and iron oxide nanoparticles at a concentration of 100 μ g/mL are dispersed in 1 mL of PBS. The cell-nanoparticle conjugates are pumped through the tube with a micro-syringe pump (Fisher Scientific, NJ) at a pulsatile flow rate of 0.1 cm/s (close to that in human body), and are captured by the micro-magnet on the internal wall of tube just underneath the X-ray source. The captured CTCs are exposed to X-rays for 10 min. The XRF peaks from bismuth nanoparticles at 10.86 and 13.02 keV are used to determine the presence of CTCs. The XRF emissions from iron oxide

nanoparticles are not used for CTC detection, because the magnet attached to the side of the tube also gives off characteristic iron peaks in the XRF spectrum. To kill captured HeLa cells through radiation induced DNA damage, the X-ray dose is increased by increasing the exposure time to 60 min and the tube voltage to 40 kV.

To evaluate the performance of our method in detecting CTCs in whole blood, the flowing PBS is replaced with human blood spiked with HeLa or MG-63 cells at a concentration of 10⁴ cells/mL. The cultured cells have been incubated for 24 h with FA conjugated bismuth nanoparticles and iron oxide nanoparticles at a concentration of 100 μ g/mL followed by PBS wash for five times before adding to the whole blood. The spiked blood samples are diluted (10 \times) with PBS to ensure a steady flow inside the tube by preventing any agglomeration or coagulation. The captured cells are exposed to X-rays for 10 min at 30 kV and 15 μ A and XRF counts for the bismuth peak at 10.86 keV are recorded. To serve as control, a background spectrum is also collected using diluted blood samples.

2.6. Comet assay

In order to test DNA damage, X-ray irradiated HeLa cells in 1 mL of 1X PBS are added into 2% low melting point agarose at a 1:1 volume ratio at 37 °C. 300 μ L of the cell-agarose suspension is dropped onto each of three 4 \times 3 cm² GelBond slides and allowed to settle at 37 °C for 10 min. The agarose is solidified by placing GelBond slides at 4 °C for 10 min. The irradiated cells are lysed by immersing slides in lysis buffer (10 mmol/L Tris–HCl, 100 mmol/L Na₂EDTA, 2.5 mol/L NaCl, 1% Triton X-100) at pH 10 and 4 °C for 1 h. The slides are placed in an electrophoresis chamber filled with alkaline buffer (0.3 mol/L NaOH and 1 mmol/L Na₂EDTA) for 40 min. The electrophoresis is carried out for 30 min by applying an 18V dc voltage across the chamber at 1 V/cm and 300 mA. Short strands of damaged DNA diffuse out of cells and migrate towards the anode. The slides are neutralized twice for 10 min in fresh buffer (0.4 mol/L Tris–HCl at pH 7.5) and stained with 5 μ g/mL of ethidium bromide (EB) aqueous solution for 30 min. The EB-labeled cells on GelBond slides are observed with epifluorescence microscope (Olympus BX51M) at magnification 10 \times and images are recorded using a computer. Images of over 100 randomly selected non-overlapping cells are analyzed for each sample using CometScore software (TriTek Corp., Sumerduck, VA).

2.7. MTT assay

X-ray irradiated HeLa cells are transferred into the microwells of a 96-well sterile microplate (BD Falcon) containing 100 μ L of media. After incubation for 24 h, the medium in each well is removed and replaced with 100 μ L of fresh culture medium. 10 μ L of the 12 mmol/L MTT stock solution is added in each well and a negative control (100 μ L of medium without nanoparticles). After incubation at 37 °C for 4 h, 100 μ L of sodium dodecyl sulfate–hydrochloric acid solution is added and mixed thoroughly using pipette. After incubating at 37 °C inside a humidified chamber for 6 h, each sample is mixed with pipette and optical absorbance at 570 nm is recorded.

2.8. Statistical analysis

Seven independent experiments ($n=7$) have been carried out for each data set and the results are expressed as mean \pm standard error of the mean (SEM). Statistical analyses were performed using SPSS 16.0 (SPSS Inc., Chicago, Illinois). One-way ANOVA and LSD tests were applied to compare the results from samples treated by different methods. $p < 0.05$ was considered statistically significant.

3. Results and discussions

3.1. Characterization of nanoparticles

Fig. 2A and B are the transmission electron microscope (TEM) images of nanoparticles made using colloidal methods, where the average diameters of bismuth nanoparticles (Fig. 2A) and iron oxide nanoparticles (Fig. 2B) are 30 and 10 nm, respectively. Fig. 2C shows DLS measurements from FA conjugated iron oxide nanoparticles in PBS with a size range of 10–45 nm and a mean diameter of 30 nm. Fig. 2C inset shows FA conjugated bismuth nanoparticles in PBS with a size range of 70–95 nm and a mean diameter of 80 nm. These results demonstrate that nanoparticles form small agglomerates, which are uniformly distributed in PBS. The FTIR spectrum in Fig. 2D for FA conjugated bismuth nanoparticles shows the presence of C–N peak ($1000\text{--}1250\text{ cm}^{-1}$) and NH_2 scissoring peaks ($1550\text{--}1650\text{ cm}^{-1}$), indicating successful conjugation of FA with bismuth nanoparticles. The conjugation of FA with iron oxide nanoparticles has also been confirmed (data not shown) using FTIR.

3.2. CTC capture and detection

Fig. 3A shows the XRF spectrum from magnetically captured HeLa cells ($\sim 1 \times 10^5$ cells/mL PBS) after exposure to X-rays for 10 min at 30 kV and 15 μA , where the peaks of bismuth L-subshell (red) from bismuth nanoparticles can be detected at 10.86 and 13.02 keV against background (black) with a SNR of ~ 5 and 2.5 respectively. The targeting specificity of FA conjugated

nanoparticles is confirmed by measuring XRF intensity of bismuth for HeLa cells and MG-63 cells. Both cell lines, after incubating with FA conjugated nanoparticles and unmodified nanoparticles, are washed five times in PBS followed by 10 min X-ray exposure at 30 kV and 15 μA . Fig. 3B shows XRF counts for the bismuth peak at 10.86 keV. HeLa cells combined with FA conjugated bismuth nanoparticles have the strongest XRF peak while HeLa cells with unmodified bismuth nanoparticles give off signal close to background (PBS control). This confirms that FA conjugated bismuth nanoparticles can combine with FRs on surface of HeLa cells through strong covalent bonds while unmodified nanoparticles are easily removed after PBS wash. To justify whether FA conjugated bismuth nanoparticles can combine with other cells, MG-63 cells are taken as a second control because of their low level of FR expression compared to HeLa cells. Results show that XRF counts from MG-63 cells, with FA conjugated nanoparticles, are at similar level as the background obtained from PBS solution. This confirms that FA conjugated nanoparticles only combine with cancer cells that over-express FRs.

The sensitivity of detection is obtained by measuring XRF signals for serially diluted CTC samples (varied from 10^2 , 10^3 , 10^4 , 10^5 CTCs/mL) in PBS. The measured XRF signals at 10.86 keV are plotted as a function of the number of CTCs per mL of PBS. Fig. 3C reveals that the detection sensitivity is ~ 100 CTCs/mL PBS for 40 min X-ray irradiation at 30 kV and 15 μA . The sensitivity can be further improved by increasing the exposure time. Fig. 3D shows the net XRF spectra (background removed) collected from HeLa cells ($\sim 1 \times 10^2$ cells/mL PBS) combined with FA conjugated nanoparticles for 20, 40, 100 and 200 min, respectively.

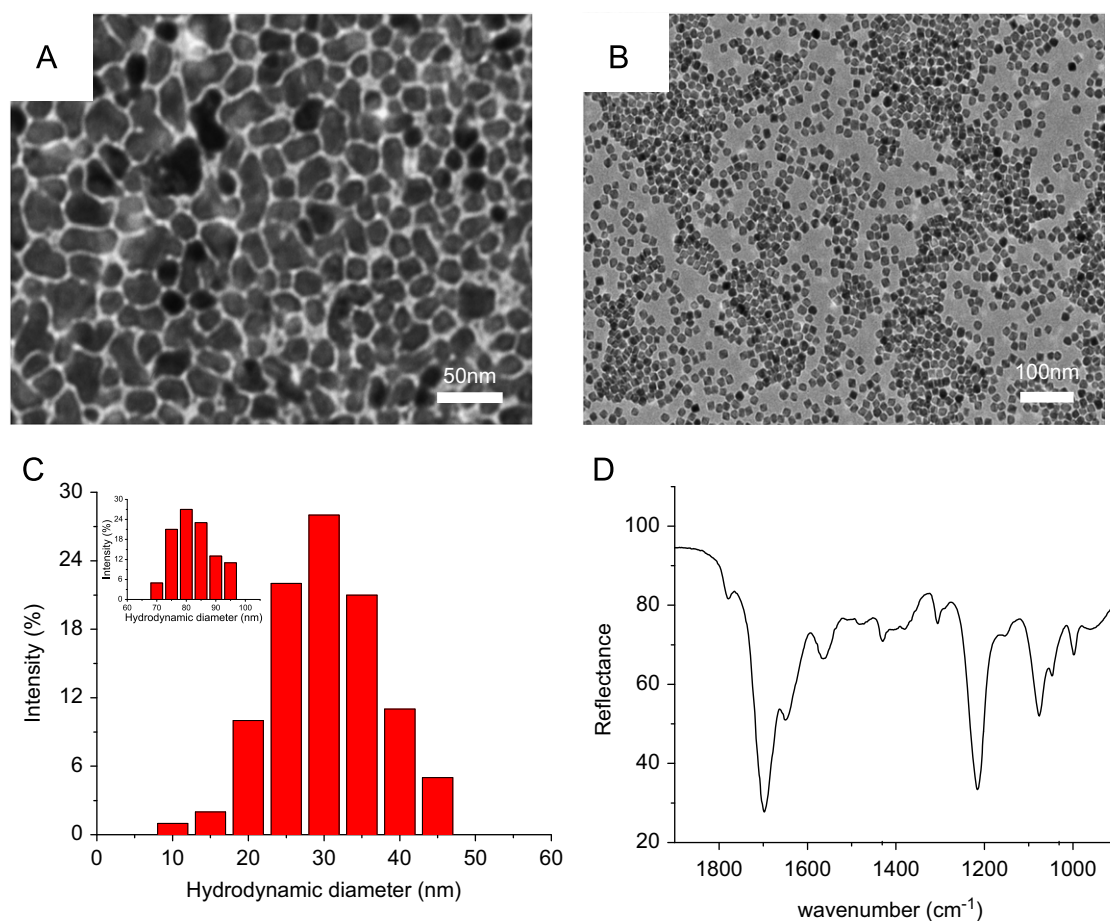


Fig. 2. Characterization of nanoparticles. TEM images of bismuth nanoparticles (A) and iron oxide nanoparticles (B); DLS measurements of iron oxide nanoparticles in PBS (inset shows bismuth nanoparticles in PBS) (C); FTIR spectrum of bismuth nanoparticles after conjugation with folic acid (D).

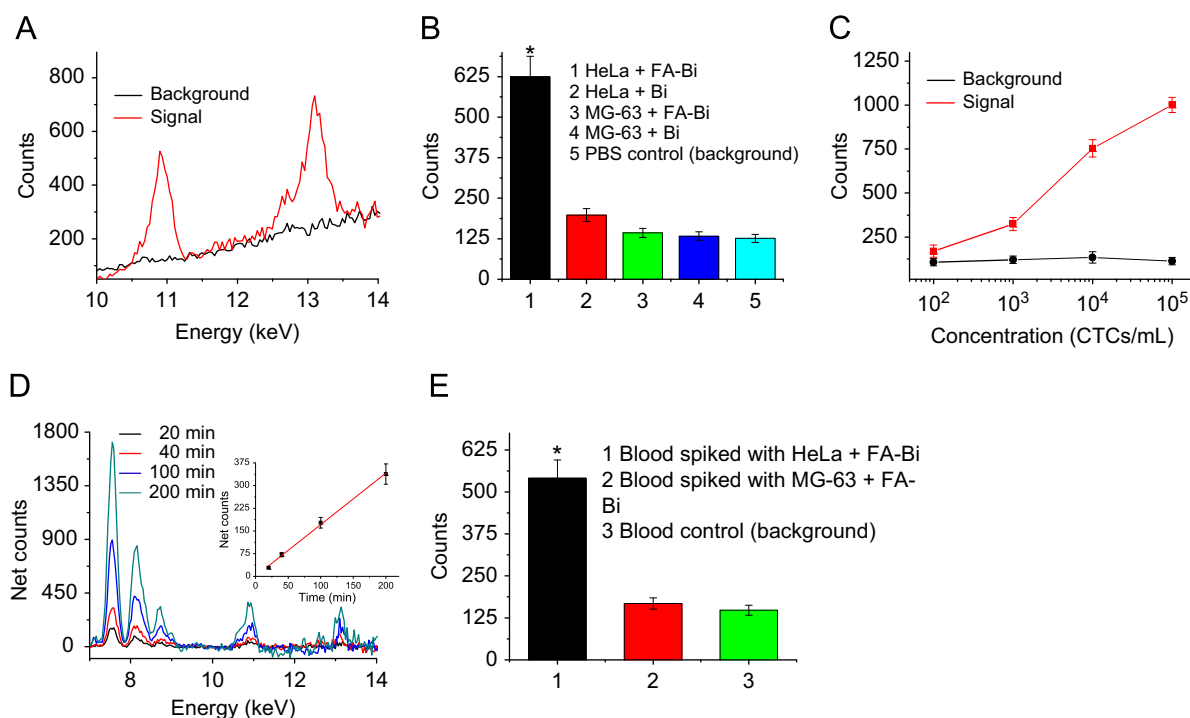


Fig. 3. CTC capture and detection. XRF spectrum obtained at 30 kV and 15 μ A after 10 min exposure of magnetically captured HeLa cells with folic acid conjugated iron oxide nanoparticles and bismuth nanoparticles (A); Bismuth XRF peak intensity at 10.86 keV of unmodified bismuth nanoparticles (Bi) and folic acid modified bismuth nanoparticles (FA-Bi) combined with HeLa cells and MG-63 cells (B), * denotes $p < 0.05$ when compared with PBS control; XRF counts for bismuth peak at 10.86 keV as a function of the number of CTCs in 1 mL PBS (C); Net XRF spectrum for HeLa cells conjugated with folic acid modified bismuth nanoparticles collected at 20, 40, 100 and 200 min using 30 kV and 15 μ A (D); XRF counts at 10.86 keV for whole blood, blood spiked with 10^4 MG-63 cells/mL, and 10^4 HeLa cells/mL, where both types of cell contain folic acid conjugated bismuth nanoparticles and iron oxide nanoparticles.* denotes $p < 0.05$ when compared with blood control (E).

Net counts at 10.86 keV are seen to increase linearly with increase in detection time (Fig. 3D inset). The sensitivity can also be enhanced if incoming X-rays can be precisely focused onto the captured CTCs and outgoing X-rays can be oriented with the detector.

The feasibility of the proposed method for clinical applications has been tested using human blood spiked with CTCs. Results show that the XRF counts at 10.86 keV for diluted blood sample is ~ 150 (background), while the corresponding values for blood samples spiked with MG-63 cells and HeLa cells are ~ 180 and ~ 550 , respectively (Fig. 3E). Although, the blood samples were spiked with high concentration of CTCs (10^4 cells/mL), the results clearly indicate the promising capabilities of the method in selectively detecting CTCs with high levels of FR expressions in whole blood.

3.3. CTC killing through radiation induced DNA damage

Nanoparticles of high atomic number elements can enhance radiation-induced damage when specifically attached on tumor cells. Specifically targeted gold nanoparticles can achieve a nucleus dose enhancement factor of up to 79 and localize ionizing energy at tumor cells, causing irreversible DNA damages that can eventually lead to cell death (Hainfeld et al., 2004; Ngwa et al., 2012; Rahman et al., 2009). Comet assay is often used to quantify DNA damage by providing complementary damage information provided by viability assays (MTT) (Karlsson, 2010; Qiao et al., 2012). The combined effect of bismuth nanoparticles and X-rays on DNA damage is studied using comet assay on magnetically captured, and X-ray irradiated HeLa cells. Since the total photoelectron cross-section of iron for 40 kVp X-rays is ~ 4 times lower than that of bismuth, the effect of iron oxide nanoparticles on X-ray induced DNA damage can be ignored. Fig. 4A shows an optical image of comets from X-ray irradiated (60 min at 40 kV

and 100 μ A) HeLa cells that have been incubated with a mixture of functionalized iron oxide nanoparticles and bismuth nanoparticles at 100 μ g/mL for 24 h. The presence of long tails means significant DNA damage. Three sets of control samples are also tested. In the first set, HeLa cells without nanoparticles are exposed to X-rays followed by electrophoresis at the same condition. Tails are observed in the resulting comets (not shown) after doing the comet assay. For the second control, HeLa cells are used that contain a mixture of functionalized nanoparticles but are not exposed to X-rays. Fig. 4B shows the absence of DNA tails from such cells after electrophoresis, suggesting that DNA damage is primarily due to X-rays and not the nanoparticles. Third set of control samples contain untreated HeLa cells without any nanoparticles or X-ray exposure. DNA damage in each sample is quantified by determining the percentage of DNA in tail (damaged) and those in entire comet (total), where the amount of DNA is derived as summation of pixel intensities in the tail or the entire comet. Fig. 4C compares the level of DNA damages, where the percentages of DNA in tails are 82.1% with X-rays and nanoparticles, 63.9% with X-rays alone, 16.9% with nanoparticles alone, and 10.1% with untreated control. In most cases, the X-ray induced DNA damages are irrecoverable, eventually leading to cell death as confirmed by other viability assays. For each set of HeLa cells mentioned above, MTT assay is carried out after incubation for 6 h following X-ray irradiation. This is done in order to confirm cell death induced by DNA damage. Fig. 4D shows the results of MTT tests where more than 80% of HeLa cells, which combined with FA conjugated nanoparticles, are killed when exposed to X-rays for 60 min at 40 kV and 100 μ A; however, only 60% HeLa cells are killed when no nanoparticles is used, suggesting the dose enhancement is provided by the X-ray absorbing nanoparticles. As for HeLa cells treated with functionalized bismuth nanoparticles but not exposed to X-rays, less

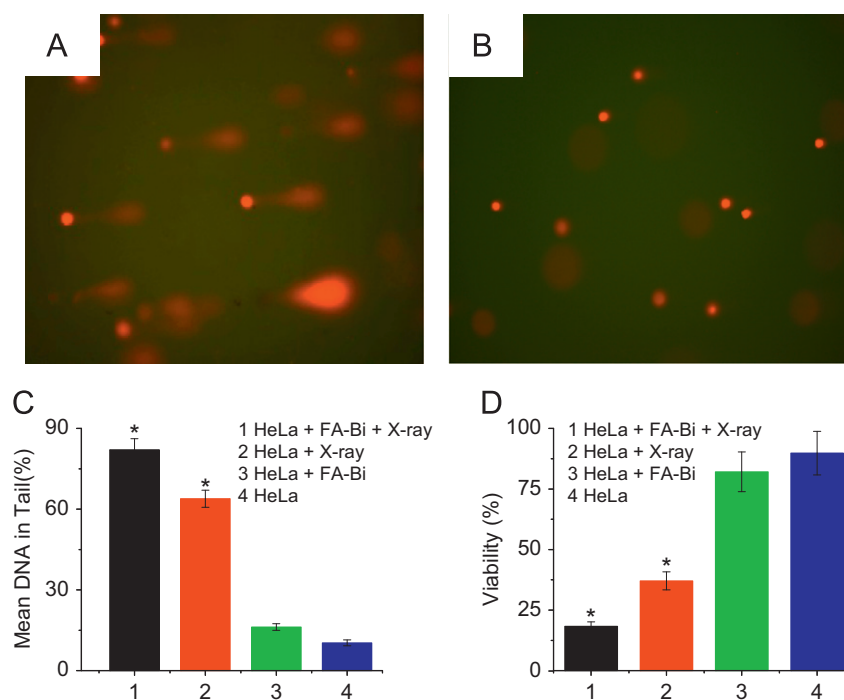


Fig. 4. CTC killing through X-ray induced DNA damage. Optical micrograph of comets from X-ray irradiated HeLa cells containing folic acid conjugated iron oxide nanoparticles and bismuth nanoparticles using 40 kV and 100 μ A X-rays for 60 min (A); Optical micrograph of comets from HeLa cells with folic acid conjugated iron oxide nanoparticles and bismuth nanoparticles without X-ray exposure (B); Mean percentage of DNA in the tail of comets under different conditions (C), * denotes $p < 0.05$ when compared with untreated control (HeLa cells); Results of MTT assay performed on HeLa cells under different conditions (D). * denotes $p < 0.05$ when compared with untreated control (HeLa cells).

than 25% cells are killed. Meanwhile, only 20% HeLa cells are dead in the untreated control. The MTT results are consistent with those from comet assay, indicating that X-rays can effectively kill captured CTCs, which can be enhanced in presence of bismuth nanoparticles.

Our results clearly indicate the potential use of XRF from targeted nanoparticles for highly selective detection and on-demand killing of CTCs in humans. However, several issues need to be considered before the method can be put to clinical use. Inherent toxicities and aggregation of both iron oxide nanoparticles and bismuth nanoparticles under *in vivo* conditions are needed to be reduced with appropriate surface coatings. For example, FA conjugated iron oxide nanoparticles that are modified with dextran and poly (ethylene glycol) (PEG), have shown enhanced stability and biocompatibility (Sonvico et al., 2005). Issues such as the circulation time of these nanoparticles and their excretion from the body should be studied using particles with different size and surface properties. Future studies will focus on the effectiveness of the proposed method under *in vivo* conditions using mice experiments.

4. Conclusion

An integrated approach that combines *in vitro* collection, detection and killing of CTCs using bismuth nanoparticles, iron oxide nanoparticles and X-ray radiation have been demonstrated. The method uses FA modified nanoparticles for selectively targeting CTCs with high levels of FR expression and offers detection capabilities as low as 100 cells/mL in a buffer solution. The detection limit can be further improved by increasing the collection time or by using X-ray focusing optics and appropriate filters to reduce background noise and increase SNR. Results also show the potential use of the technique for detecting CTCs in whole blood, indicating future clinical applications. Use of X-rays allows

simultaneous detection and eradication of CTCs, thus, providing a novel strategy for management of cancer metastasis.

Acknowledgments

This project has been supported by a research grant (0828466), and a Faculty Early Career Development Award (CAREER) from the National Science Foundation, as well as a Concept Award from Lung Cancer Research program of the Congressionally Directed Medical Research Program of Department of Defense.

References

- Benez, A., Geiselhart, A., Handgretinger, R., Schiebel, U., Fierbeck, G., 1999. Journal of Clinical Laboratory Analysis 13, 229–233.
- Bhattacharya, D., Das, M., Mishra, D., Banerjee, I., Sahu, S.K., Maiti, T.K., Pramanik, P., 2011. Nanoscale 3, 1653–1662.
- Bilkenroth, U., Taubert, H., Riemann, D., Rebmann, U., Heynemann, H., Meye, A., 2001. International Journal of Cancer 92, 577–582.
- Chung, Y.K., Reboud, J., Lee, K.C., Lim, H.M., Lim, P.Y., Wang, K.Y., Tang, K.C., Ji, H., Chen, Y., 2011. Biosensors and Bioelectronics 26, 2520–2526.
- Dharmasiri, U., Njoroge, S.K., Witek, M.A., Adebisi, M.G., Kamande, J.W., Hupert, M.L., Barany, F., Soper, S.A., 2011. Analytical Chemistry 83, 2301–2309.
- Galantha, E.I., Shashkov, E.V., Kelly, T., Kim, J.W., Yang, L., Zharov, V.P., 2009. Nature Nanotechnology 4, 855–860.
- Gascoyne, P.R., Noshari, J., Anderson, T.J., Becker, F.F., 2009. Electrophoresis 30, 1388–1398.
- Georgakoudi, I., Solban, N., Novak, J., Rice, W.L., Wei, X., Hasan, T., Lin, C.P., 2004. Cancer Research 64, 5044–5047.
- Gutierrez-Juarez, G., Gupta, S.K., Weight, R.M., Polo-Parada, L., Papagiorgio, C., Bunch, J.D., Viator, J.A., 2010. International Journal of Thermophysics 31, 784–792.
- Hainfeld, J.F., Slatkin, D.N., Smilowitz, H.M., 2004. Physics in Medicine and Biology 49, N309–N315.
- Hatzistavros, V.S., Koulouridakis, P.E., Aretaki, I.I., Kallithrakas-Kontos, N.G., 2007. Analytical Chemistry 79, 2827–2832.
- He, W., Wang, H.F., Hartmann, L.C., Cheng, J.X., Low, P.S., 2007. Proceedings of the National Academy of Sciences of the USA 104, 11760–11765.
- Heimann, R., Hellman, S., 2000. Journal of Clinical Oncology 18, 591–599.
- Hossain, M., Wang, C., Su, M., 2010. Applied Physics Letters 97, 263704.

- Hsieh, H.B., Marrinucci, D., Bethel, K., Curry, D.N., Humphrey, M., Krivacic, R.T., Kroener, J., Kroener, L., Ladanyi, A., Lazarus, N., Kuhn, P., Bruce, R.H., Nieva, J., 2006. *Biosensors and Bioelectronics* 21, 1893–1899.
- Hu, Y., Fan, L., Zheng, J., Cui, R., Liu, W., He, Y., Li, X., Huang, S., 2010. *Cytometry A* 77, 213–219.
- Kaiser, J., 2010. *Science* 327, 1072–1074.
- Karlsson, H.L., 2010. *Analytical and Bioanalytical Chemistry* 398, 651–666.
- Kojima, T., Hashimoto, Y., Watanabe, Y., Kagawa, S., Uno, F., Kuroda, S., Tazawa, H., Kyo, S., Mizuguchi, H., Urata, Y., Tanaka, N., Fujiwara, T., 2009. *Journal of Clinical Investigation* 119, 3172–3181.
- Lin, H.K., Zheng, S., Williams, A.J., Balic, M., Groshen, S., Scher, H.I., Fleisher, M., Stadler, W., Datar, R.H., Tai, Y.C., Cote, R.J., 2010. *Clinical Cancer Research* 16, 5011–5018.
- Liu, M.C., Shields, P.G., Warren, R.D., Cohen, P., Wilkinson, M., Ottaviano, Y.L., Rao, S.B., Eng-Wong, J., Seillier-Moisewitsch, F., Noone, A.M., Isaacs, C., 2009. *Journal of Clinical Oncology* 27, 5153–5159.
- Mann, S.E., Ringo, M.C., Shea-McCarthy, G., Penner-Hahn, J., Evans, C.E., 2000. *Analytical Chemistry* 72, 1754–1758.
- Nagrath, S., Sequist, L.V., Maheswaran, S., Bell, D.W., Irimia, D., Utkus, L., Smith, M.R., Kwak, E.L., Digumarthy, S., Muzikansky, A., Ryan, P., Balis, U.J., Tompkins, R.G., Haber, D.A., Toner, M., 2007. *Nature* 450, 1235–1239.
- Nedosekin, D.A., Sarimollaoglu, M., Shashkov, E.V., Galanzha, E.I., Zharov, V.P., 2010. *Optics Express* 18, 8605–8620.
- Neugebauer, U., Bocklitz, T., Clement, J.H., Krafft, C., Popp, J., 2010. *Analyst* 135, 3178–3182.
- Nezos, A., Msaouel, P., Pissimissis, N., Lembessis, P., Sourla, A., Armakolas, A., Gogas, H., Stratigos, A.J., Katsambas, A.D., Koutsilieris, M., 2011. *Cancer Treatment Reviews* 37, 284–290.
- Ngwa, W., Makrigiorgos, G.M., Berbeco, R.I., 2012. *Medical Physics* 39, 392–398.
- Pantel, K., Brakenhoff, R.H., Brandt, B., 2008. *Nature Reviews Cancer* 8, 329–340.
- Qiao, Y., Wang, C., Su, M., Ma, L., 2012. *Analytical Chemistry* 84, 1112–1116.
- Rabin, O., Manuel Perez, J., Grimm, J., Wojtkiewicz, G., Weissleder, R., 2006. *Nature Materials* 5, 118–122.
- Rahman, W.N., Bishara, N., Ackerly, T., He, C.F., Jackson, P., Wong, C., Davidson, R., Geso, M., 2009. *Nanomedicine* 5, 136–142.
- Sha, M.Y., Xu, H., Natan, M.J., Cromer, R., 2008. *Journal of the American Chemical Society* 130, 17214–17215.
- Sonvico, F., Mornet, S., Vasseur, S., Dubernet, C., Jaillard, D., Degrouard, J., Hoebeke, J., Duguet, E., Colombo, P., Couvreur, P., 2005. *Bioconjugate Chemistry* 16, 1181–1188.
- Sun, Y.F., Yang, X.R., Zhou, J., Qiu, S.J., Fan, J., Xu, Y., 2011. *Journal of Cancer Research and Clinical Oncology* 137, 1151–1173.
- Wang, S., Liu, K., Liu, J., Yu, Z.T., Xu, X., Zhao, L., Lee, T., Lee, E.K., Reiss, J., Lee, Y.K., Chung, L.W., Huang, J., Rettig, M., Seligson, D., Duraiswamy, K.N., Shen, C.K., Tseng, H.R., 2011a. *Angewandte Chemie International Edition* 50, 3084–3088.
- Wang, X., Qian, X., Beitler, J.J., Chen, Z.G., Khuri, F.R., Lewis, M.M., Shin, H.J., Nie, S., Shin, D.M., 2011b. *Cancer Research* 71, 1526–1532.
- Weight, R.M., Viator, J.A., Dale, P.S., Caldwell, C.W., Lisle, A.E., 2006. *Optics Letters* 31, 2998–3000.
- Wulfskuhle, J.D., Liotta, L.A., Petricoin, E.F., 2003. *Nature Reviews Cancer* 3, 267–275.
- Yu, M., Stott, S., Toner, M., Maheswaran, S., Haber, D.A., 2011. *Journal of Cell Biology* 192, 373–382.
- Zborowski, M., Chalmers, J.J., 2011. *Analytical Chemistry* 83, 8050–8056.
- Zemp, R.J., 2009. *Nature Nanotechnology* 4, 798–799.
- Zhang, Y., Kohler, N., Zhang, M.Q., 2002. *Biomaterials* 23, 1553–1561.
- Zharov, V.P., Galanzha, E.I., Shashkov, E.V., Khlebtsov, N.G., Tuchin, V.V., 2006. *Optics Letters* 31, 3623–3625.
- Zheng, S., Lin, H., Liu, J.Q., Balic, M., Datar, R., Cote, R.J., Tai, Y.C., 2007. *Journal of Chromatography A* 1162, 154–161.
- Zheng, S., Lin, H.K., Lu, B., Williams, A., Datar, R., Cote, R.J., Tai, Y.C., 2011. *Biomedical Microdevices* 13, 203–213.